Iraqi Geological Journal

Journal homepage: https://www.igj-iraq.org

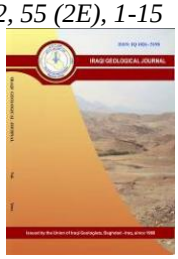

Paleostress Determination and Structural Analysis of the Area between Amman and Qasr Al-Hallabat, North Jordan

Masdouq Al-Taj[1,*], Sumaia Yasin [2] and Abdullah Diabat [3]

[1] Department of Earth and Environmental Sciences, Prince El Hassan Bin Talal Faculty for Natural Resources and Environment, The Hashemite University, Zarqa 13133, Jordan
[2] International Pioneers Academy, Amman, Jordan
[3] Department of Applied Earth and Environmental Sciences, Faculty of Earth and Environmental Sciences, Al al-Bayt University, Mafraq, Jordan
* **Correspondence**: maltaj@hu.edu.jo

Received:
13 May 2022

Accepted:
11 August 2022

Published:
30 November 2022

Abstract

This research derives paleostress tensors for deformation affecting late Cretaceous rocks between Amman and Al-Hallabat, northern Jordan and reconstructs the region's tectonic history. Three distinct formations are exposed in the investigated area: Wadi As Sir (Turonian), Wadi Umm Ghudran (Santonin), and Amman silicified limestone (Campanian). The stress inversion is derived from data collected on the fault-slip at four different locations, revealing both extensional and compressive regimes. The research region is divided into two sectors based on these paleostress regimes: a SW sector dominated by extensional to transtensive stress regimes (with a stress index varying from 0.68 to 0.80) and a NE sector characterized by compression (with a stress index ranging from 2.60 to 2.65). Furthermore, the SE stress sector is found to be consistent with the NNW-SSE Neogene extension. In contrast, the NE stress sector was associated with a Syrian Arc Stress Field orientated E-W to ESE-WNW throughout the late Cretaceous. Fracture analysis identifies two types of fractures within the study area: shear and extensional. Both fractures correspond with fault-slip data and inferred stress direction.

Keywords: Amman-Hallabat structure; Paleostress analysis; Tensor program; Transpression; Transtension

1. Introduction

Cretaceous rocks represent around sixty percent of Jordan's outcropped rocks (Abed, 2017). The thickness decreases from the north to the south and from the west to the east. In Jordan, two Cretaceous sedimentation facies are recognized, with sandstone dominating the Early Cretaceous and limestone dominating the Late Cretaceous. Early Cretaceous sandstone overlies the Jurassic and Triassic in northern and central Jordan, and the Silurian, Ordovician, and Cambrian in southern Jordan. The majority of the carbonaceous rocks of the Late Cretaceous consist of limestone, marl, marly limestone, chalk, chert, and phosphate.

Previous geological studies in the northern part of Jordan have identified the general structural framework (Mikbel and Zacher, 1981; Atallah and Mikbel, 1992; Abed, 2017), but no detailed investigations of the structures, particularly in the Zarqa area, have been carried out.

DOI: 10.46717/igj.55.2E.1ms-2022-11-15

Paleostress analysis offers much information about the structural history of a particular region and can shed a light on the deformation processes within different lithologies. It aims to establish the magnitude and orientation of the stress field in which a population of faults and fractures are created (e.g., Rowland et al., 2007; Zain Eldeen et al., 2002; Radaideh and Melichar, 2015; Soumaya et al., 2018; Al-Shwaily and Al-Obaidi 2019; Tiwari et al., 2020). Several hypotheses have been presented to explain the structural styles of the Dead Sea Transform's eastern side (DST). Some researchers relate the structural formation to the Arabian plate's northward sliding along the DST since the M. Miocene (Atallah, 1992; Ferry et al., 2007; Garfunkel, 2014; Abutaha et al., 2019), and additional insights come from current research on continental strike-slip faults, which document the characteristic arrangements of tectonic features such as pressure ridges, sag ponds, horsetail structures, and splay faults (Al-Taj et al., 2004; Al Hseinat et al., 2020). Other researchers, however, explain the same structures as part of the Syrian Arc fold belt, which formed in the Late Cretaceous to the M. Miocene (Eyal, 1996). Al-Khatib et al. (2010) conducted stress studies in northern Jordan and found faulting consistent with both the Syrian Arc and the Dead Sea stress fields (SAS and DSS respectively).

Faulting is the most prominent structural feature in the north Jordan area, with the most distinctive structures being the ENE-WSW-striking Amman-Hallabat fault systems (AHF) and the E-W trending Birin Fault (Fig. 1). In the eastern part of the study area, these two faults converge and intersect close to Qasr Al Hallabat, producing a graben border. The aim of this research was to reconstruct the paleostress tensors that influenced Late Cretaceous rocks and thereby clarify the tectonic history of Jordan's northwestern region, specifically the area located between Amman and Al-Hallabat (Fig. 1). The study area (bordered by the coordinates: long. 35˚ 56′ - 36˚ 20’ E and lat. 31˚ 56’ - 32˚ 07’ N) is easily accessible via the Free Zone Area highway and a new highway that is locally called the 100 highway.

2. Geological Setting

2.1 Stratigraphy

The lithostratigraphy of the studied successions includes the following Formations, discussed below from oldest to youngest (Fig. 1):

2.1.1. Shueib Formation (S)

This Formation is underlaind by thick-bedded dolomitic limestones of the Hummar Formation and overlain by massive, bedded carbonates of the Wadi As Sir Limestone Formation. The exposed part of this formation in the study area does not exceed 10 m in its thickness in some parts, and it is not exposed in others. Its age is Early Turonian (Fig. 1), and it comprises thin-bedded, buff to grey limestone with marl intercalation in its lowest part (Abu-Qudaira, 2001).

2.1.2. Wadi As Sir Limestone Formation (WSL)

This Turonian age unit is around 80 meters thick (Fig. 1) and consists of three units. Dolomitic limestone, dolomite, and recrystallized calcareous beds characterize the bottom unit. Soft marly limestone and limestone beds make up the middle unit, while thick massive limestone makes up the upper unit. In the upper and intermediate units, nodules and chert beds are common (Abed, 2017; Farouk et al., 2017).

2.1.3. Wadi Umm Ghudran Formation (WG)

This is a soft lithology of yellow to white-gray chalky limestones and limestones, Santonian in age (Abed, 2017), and with up to 12 m exposed thickness (Fig. 1).

2.1.4. Amman silicified limestone formation (ASL)

This Early Campanian unit (Abed, 2017) has an outcrop thickness of about 40 m and consists of a thin to medium bedded grey, white, or brown chert, silicified limestones, limestones and a phosphatic chert bed at the top. Undulating bedding characterizes the formation, which becomes increasingly obvious in Amman and is not thought to be tectonic in origin (Masri, 1963).

2.*1.5. Al Hisa Phosphorite Formation (AHP)*

Thin- to medium-bedded phosphates, limestones, cherty phosphates, marls, and coquinas constitute the (Campanian-Maastrichtian) Al Hisa Formation, which is 30 m thick.

2.1.6. Superficial deposits (SD)

The Quaternary superficial deposits can be differentiated into ‘soil’, ‘alluvial sediments’ and ‘wadi sediments’ (Fig. 1). According to Abu-Qudaira (2001),'soil' is thick, dark to pale brown in tone, and is associated with basalt clasts in the northern portion of the research region. Holocene alluvial and wadi sediments are found in floodplains.

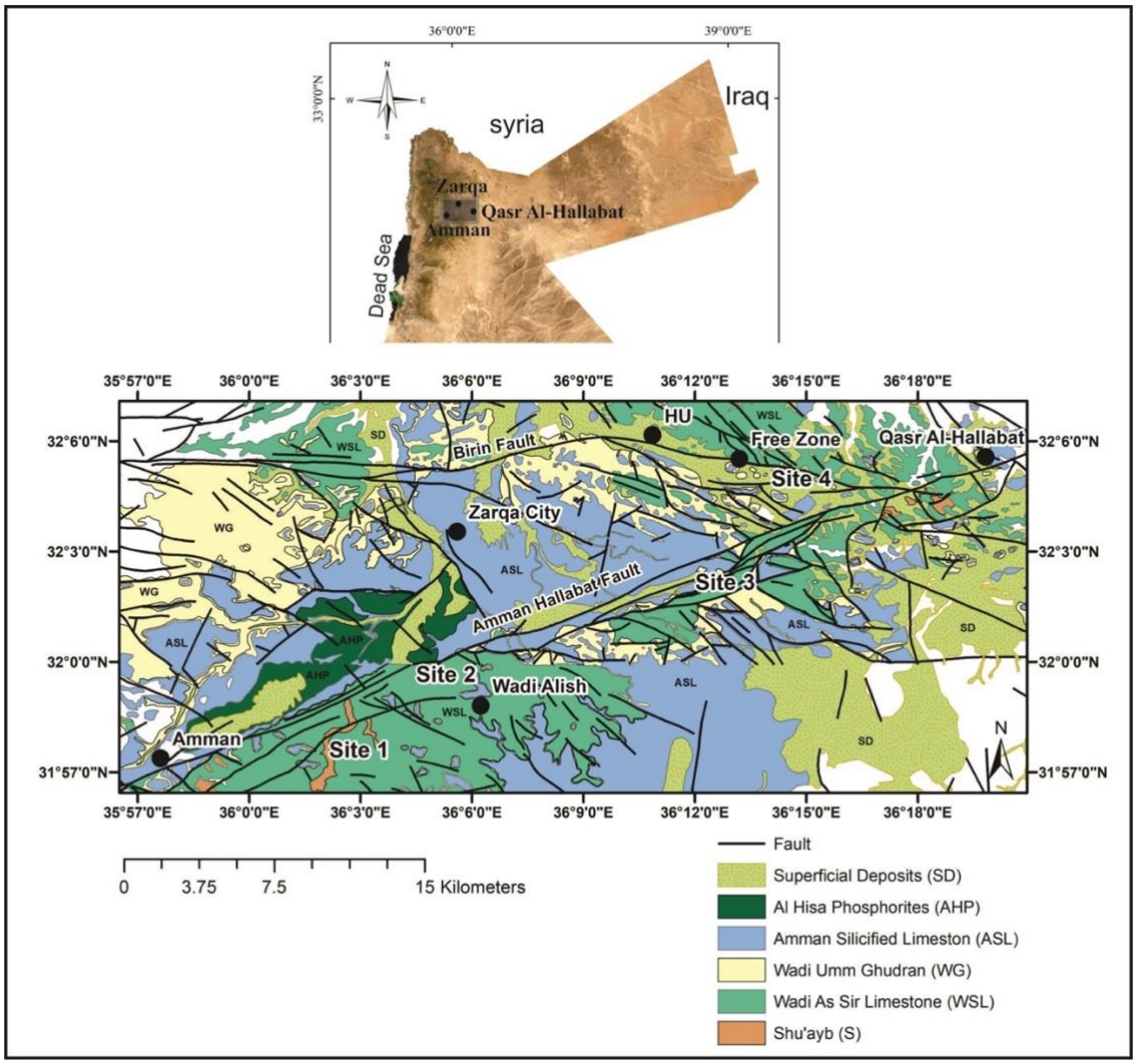

Fig. 1. Location and geological map of the study area compiled from Sahab sheet map of Faddah (1988); Zarqa sheet map of Abu-Qudaira (2001); Qasr Al-Hallabat sheet map of Al Hiyari (2004); Amman sheet map of Diabat and Abdelghafoor (2004).

2.2. Structural and Tectonic Setting

According to Quennell (1959), the major tectonic structures in Jordan were formed by three stress fields. These stress fields have been operating in Jordan since the Late Cretaceous period, running from the NE-SW to the ENE to the E-W directions. From the late Cretaceous to the Miocene, Jordan was significantly affected by tectonic stresses associated with the opening of the Red Sea and the northward movement of the Arabian Plate and Palestine-Sinai subplate. During that period, Jordan was located at the southern border of the Neo-Tethys Ocean. At the boundaries of the Arabian Plate, a heavy accumulation of sediment developed (Farouk et al., 2017). Consequently, Jordan is a region that experienced major tectonic events that began in the Late Cretaceous and generated basins and swells associated with the main tectonic pulses of the Syrian Arc Fold Belt during the Late Cretaceous (Farouk et al., 2014; Ahmad et al., 2014).

The Dead Sea Transform (DST) is the main tectonic structure that accommodates the Arabian plate's faster northward movement than the African plate (Garfunkel, 1981; Galli, 1999; Weber et al., 2014; Farouk et al., 2016) (Fig. 2). The DST in Jordan is composed of the Wadi Araba Fault (WAF) in the south and the Jordan Valley Fault (JVF) in the north. Due to the formation of the Red Sea, the Arabian plate rotated 5.5 degrees clockwise in regard to the Sinai-Palestine microplate, with fault movement initiating since M. Miocene (Garfunkel, 1997, Garfunkel, 2014). Horizontal fault displacement, estimated to be 107 km, occurred in two phases: 62 km of slip during the M. Miocene and 45 km of slip during the Late Pliocene-Early Pleistocene (Quennell, 1958). The Amman-Hallabat Structure (AHS) is an important sinistral subsidiary fault of the DST at its western part. The (AHS) cut across the research area, striking ENE-WSW from Amman to Qasr Al-Hallabat (Fig. 1).

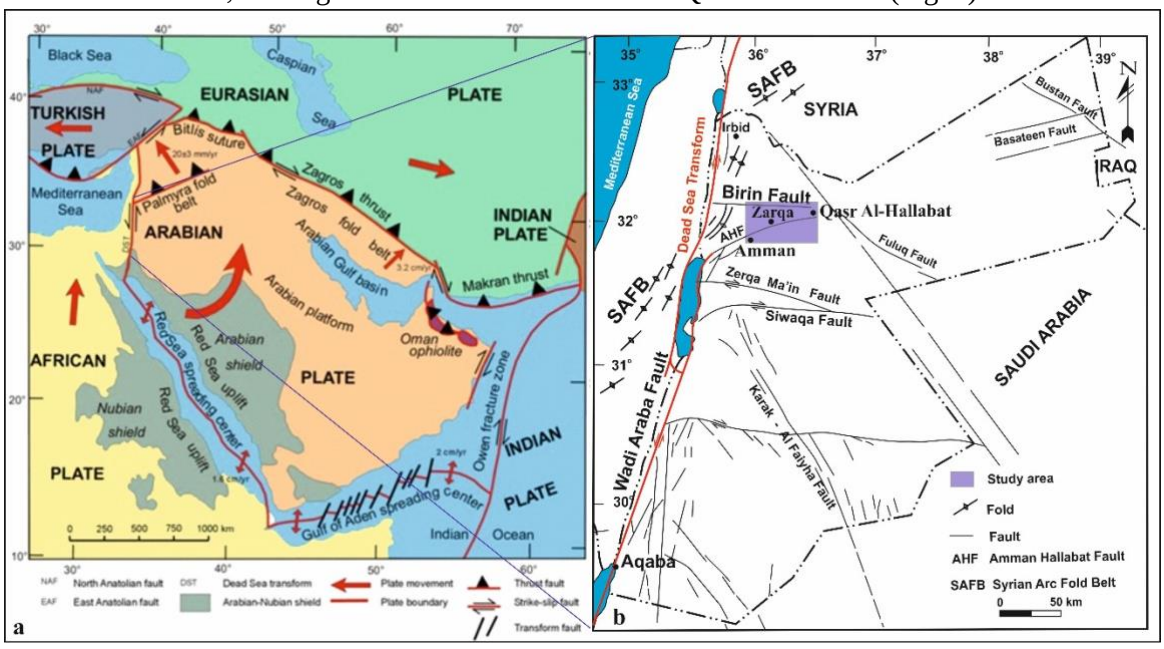

Fig. 2. Structural setting of the study area; a) The boundaries of the Arabian Plate relative. to its neighboring plates (modified from Abd, 2021); b) Structural pattern of Jordan showing the location of the study area (modified from Diabat and Masri, 2005).

Mikbel and Zacher (1986) created the term "Amman-Hallabat Structure" (AHS) to describe the main structure crossing the study area (Fig. 1). They considered AHS as a fault and fold-bending faults system, starting from the NE end of the DST east of the Dead Sea, and striking in an ENE direction towards Amman, curving E-W near Zarqa city until it is buried below the basaltic flows in the Qasr Al-Hallabat area northeast of Zarqa (Figs. 1 and 2). The AHS is thought to have formed as a result of compressive stresses caused by the Arabian plate's northward migration (Atallah and Mikbel, 1992).

Diabat (2009) proposed reactivation of this structure along numerous minor fault planes affecting Neogene strata. The AHS may have been renewed in the Quaternary (Alawabdeh et al., 2016), possibly as horsetail faults at the end of the (WAF) (Al Hseinat et al., 2020). According to this interpretation, the AHS has been reactivated as a restraining bend, part of an active strike-slip fault segment created by the NNW-SSE trending (DSS) (Al Hseinat et al., 2020).

3. Materials and Methods

A detailed study was undertaken in the area, using four field sites to collect the structural data, including fault planes, slickensides measurements and joint systems (Fig. 1). In the four sites, field measurements are carried out at 12 field stations that stretch from the NE of Amman through the Hashemite University and along to the east of the Free Zone Area. The quantity and quality of the structural information vary along this study corridor. In some stations, few faults or slickensides are found, and in others passing through military camps in the NE part of the research area, no photography of the field site is allowed. The measurements are collected from WSL and ASL Formations in which the associated strata crop out in sufficient thickness. Measurements of fault slips were obtained at twelve field stations throughout four sites in the study area (quarries, road cuts, and wadi exposures) and are labeled S1 to S12 (Figs. 1 and 3). As many as possible fault planes, joints and slickensides were measured in each station. Based on kinematic indicators e.g., relative displacement and slickensides, the faults encountered in the research area varied from normal, strike-slip and oblique-slip faults (Fig. 5). Due to a lack of data at some sites, and because some of the data collected at adjacent stations were very similar, the stations were grouped into four sites that showed a common stress regime. The first site includes S1, S2, S3 and S4, the second site includes S5 and S6, the third site involves S7, S8 and S9, and finally, the fourth site involves stations S10, S11 and S12 (Fig. 3). In this study, the latest version of Rockwork was used (Rockwork 17) to analyze the joint data that were taken in the field at different stations and present the results as rose diagrams showing the number of joint sets and their general trends. Fault-slip data were analyzed by using the Tensor program within the paleostress software, an efficient and standard software for determining tectonic stress of the geological fault-slip data and earthquake fault-plane solution in structural geology, including seismotectonic and neotectonics investigations.

The fault-slip analysis process using an enhanced version of the TENSOR software (Delvaux and Sperner, 2003; Delvaux, 2011) allowed the derivation of the principal stress axes (σ1, σ2 and σ3), and hence the overall paleostress regime in the research area. The stress inversion techniques are based on the premise that slip develops along the fault plane in the direction of the greatest resolved shear stress (Bott, 1959). The inversion of the fault-slip data offers four parameters relating to the reduced stress tensor. These are; σ1, σ2 and σ3, and the stress ratio $R=(\sigma2-\sigma3)/(\sigma1-\sigma3)$. It also computes the S_{Hmax}, which represents the horizontal maximum principal stress axis, and the S_{hmin}, which denotes the horizontal minimum principal stress axis (Angelier, 1994; Delvaux et al., 1995). The stress regime type is expressed numerically using the stress index (R'), which ranges from 0 to 3 (Fig. 4). The index R' emphasizes the stress regime entirely and efficiently finds the regional stress regime generated from different individual stress tensors within a particular region.

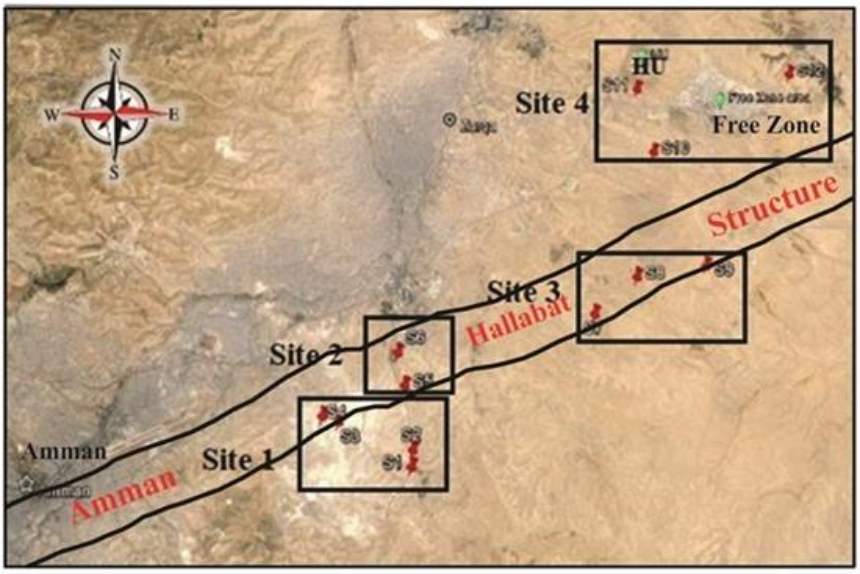

Fig. 3. Location map for field sites and stations superimposed on Google Earth photo. HU is The Hashemite University.

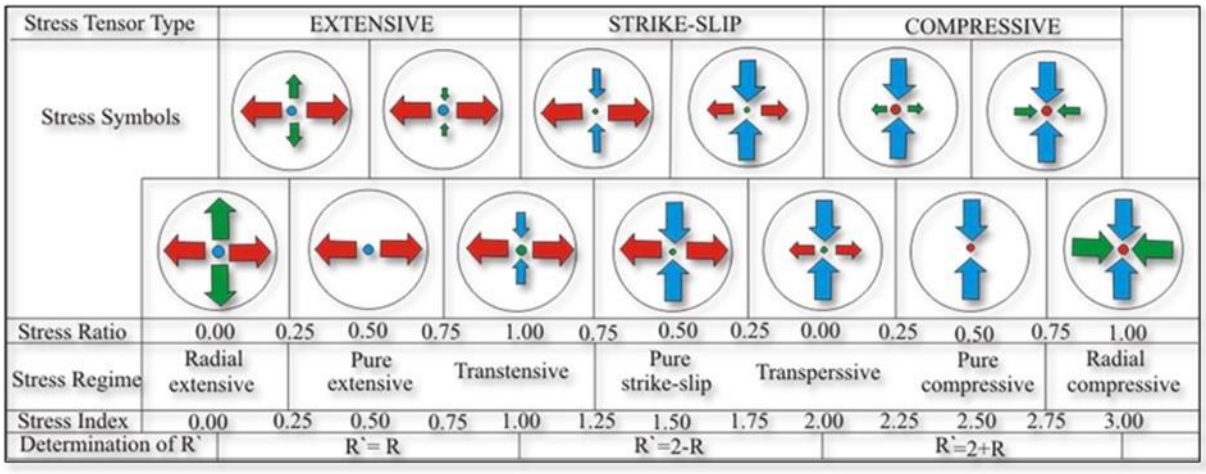

Fig. 4. Types of stress regimes and their representation in map view (after Guiraud et al., 1989).

4. Results

The following is a representation of the results in each station:

4.1. Site 1

Site 1 includes four stations in the SW part of the research area (Fig. 3). In the first station (S1) (31° 57' 47.50" N and 36° 5' 34.9" E) many fault planes are easily recognized on roadsides, with the majority being normal faults (Fig. 5a). Station S2 (31° 58' 6" N and 36° 5' 36.10" E) at the Wadi Alish area, close to station S1, also exhibits largely normal faults. Station S3 (31° 58' 34.40" N and 36° 3' 50.8" E) in a quarry in the Wadi Alish area is similarly dominated by normal faults (Fig. 5). Station S4 (31° 58' 39.70" N and 36° 3' 27.2" E) also at the quarry site in the Wadi Alish area displays faults with oblique and horizontal slickenlines (Fig. 5d). The obtained results of the calculated principal stresses in site 1 are shown in Fig. 6 and Table 1.

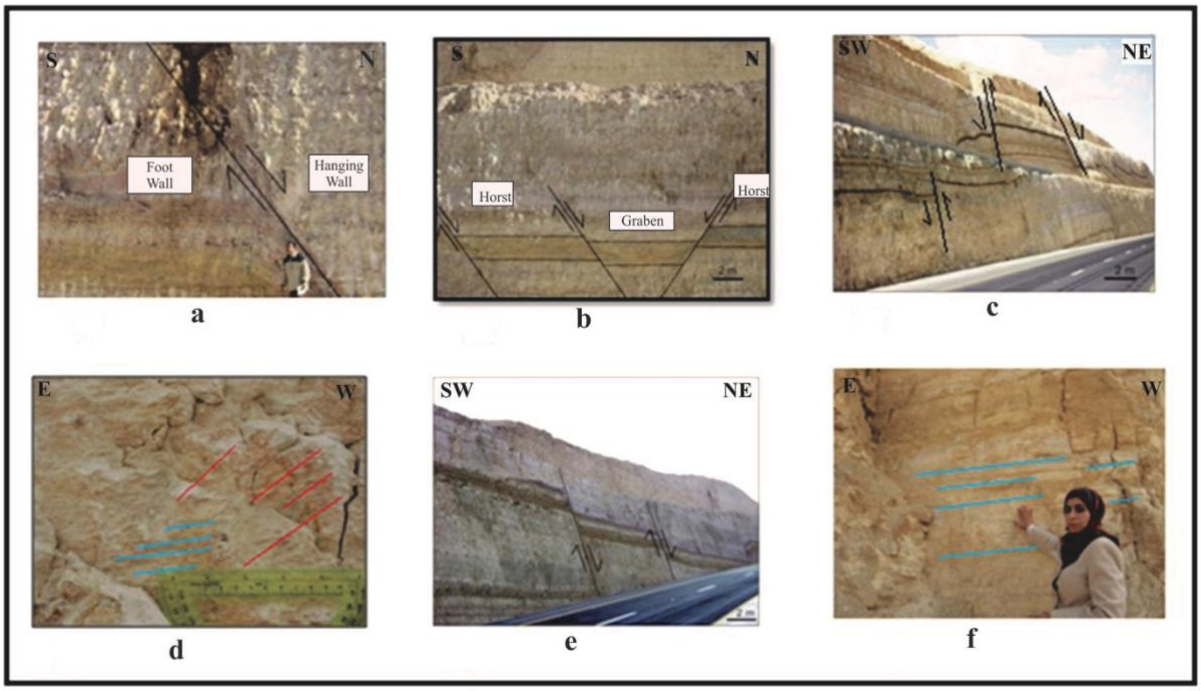

Fig. 5. Examples of kinematic indicators in different stations of the study area; (a) normal fault in station S1; (b) graben structure in station S5; (c) horst structure and vertical faults in station S6; (d) two generations of faults based on slickenlines horizontal blue and oblique red in station S4,;(e) step normal faults in station S5, and (f) horizontal slickenlines in station S12.

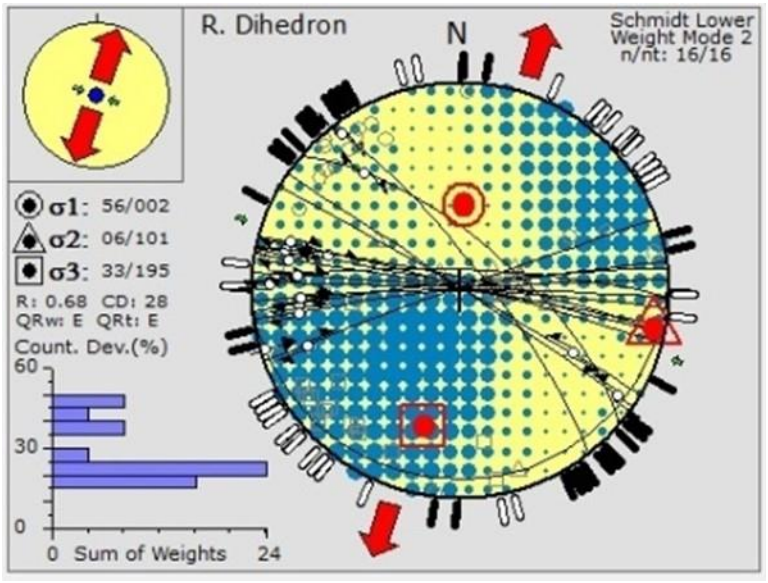

Fig. 6. Stress inversion result for site 1.

Table 1. A summary of the paleostress tensors in the study area

Site No.	R	R'	S_{Hmax}/S_{hmin}	Principal Stresses			Type of Tensor	Fm.
				σ_1	σ_2	σ_3		
1	0.68	0.68	195 S_{hmin}	56/002	06/101	33/195	pure Extensive to Transtensive	WSL
2	0.80	0.80	209 S_{hmin}	51/017	06/114	39/209	Transtensive	WSL and ASL
3	0.65	2.65	093 S_{Hmax}	24/093	18/355	59/231	pure compressive	WSL
4	0.60	2.60	089 S_{Hmax}	04/089	11/358	78/198	pure compressive	WSL

4.2. Site 2

The SW part of the research area includes stations S5 and S6. Station S5 (31° 59' 17.7" N and 36° 5' 21.30" E) is about 4 km from Amman-Zarqa Highway (Fig. 3) and shows many faults or fault zones. Horst and graben system (Fig. 5b) and step faults (Fig. 5e) are detected. About 2 km north of S5 is station S6 (31° 59' 55.1" N and 36°5' 9.80" E) where numerous oblique normal faults are observed in a road section outcrop, including a wide range of step faults and horst structures (Fig. 5c). The stress inversion result for Site 2 is shown in Fig. 7 and Table 1.

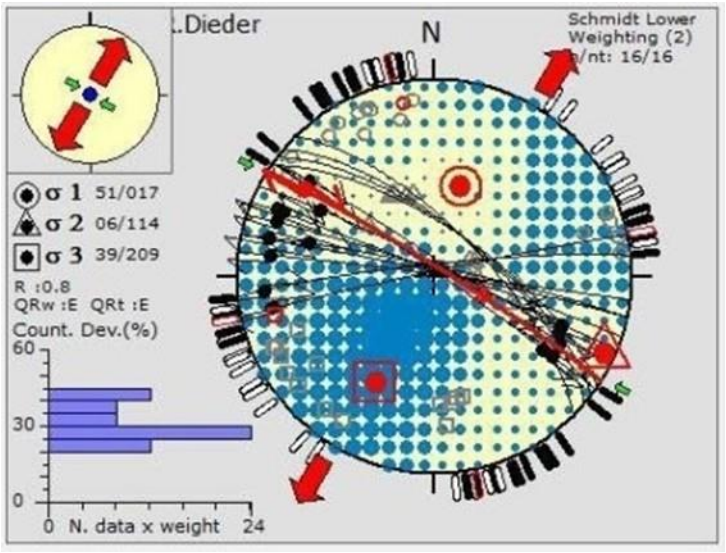

Fig. 7. Stress inversion result for stations S5 and S6 of site 2.

4.3. Site 3

Stations S7, S8, and S9 are located in the northeastern side of the research area. Several fault planes are visible at station S7 (32° 0' 47.0" N and 36° 9' 51.7" E) but no photo is available due to the security factors that the adjacent military camp requires. About 2 km NE from S7, outside the military camp, lies S8 (32° 1' 32.3" N and 36° 10' 35.7" E) where faults here and at nearby S9 (32° 1' 47.7" N, and 36° 12' 34.3" E) show a compressive stress regime (Fig. 8a). The determined major stresses for Site 3 are shown in Table 1 based on the fault-slip data. Additionally, this site is highly jointed, and 140 joints were measured at Station S9. The generated rose diagram represents a major NW-SE trend and a minor ENE-WSW trend (Fig. 8b).

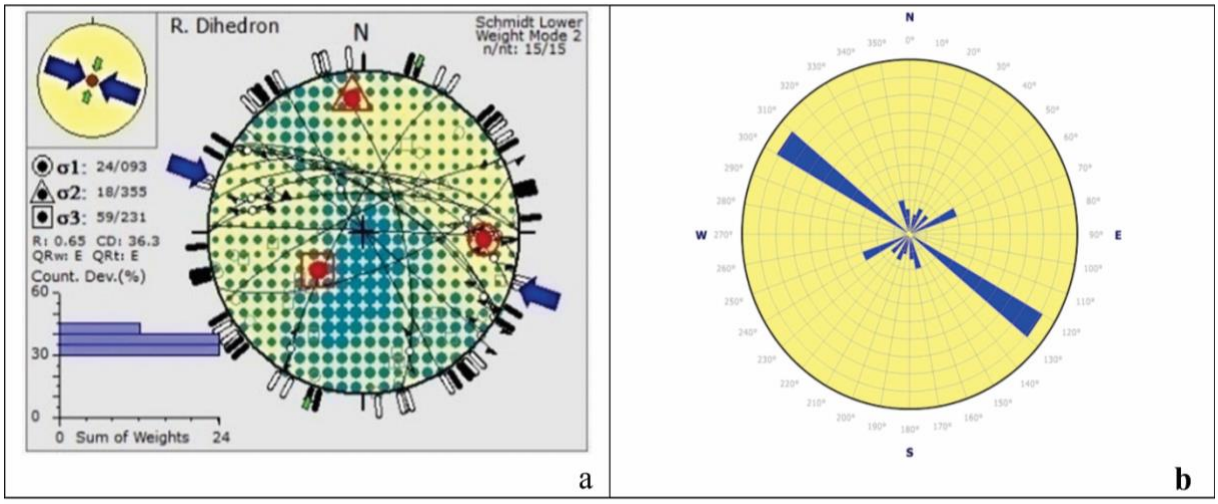

Fig. 8. (a) Stress inversion result for site 3; (b) Rose diagram of 140 joints in station S9.

4. 4. Site 4

Field stations S10, S11, and S12 are located to the northeast of the research area (Fig. 3). Station S10 (32° 4' 7.15" N and 36° 11' 22.6") is about 4 km south of the Hashemite University whilst station S11 (32° 5' 28.7" N and 36° 11' 0.1" E) is in the vicinity of the Hashemite University (Southern Gate). Station S12 (32° 5' 53.2" N and 36° 14' 53.7" E) in the old quarry site northeast of the Free Zone Area (Figs. 1 and 3). The fault-slip data analysis for the stations in this area reveals a compressive stress regime (Fig. 9). The obtained results of the calculated principal stresses are shown in Table 1. Joints are measured in Stations S11 and S12 with a total of 180 and 150, respectively (Fig. 10). Rose diagrams show E-W major and NW-SE minor trends in S11 and NW-SE major trend in S12 (Fig. 10).

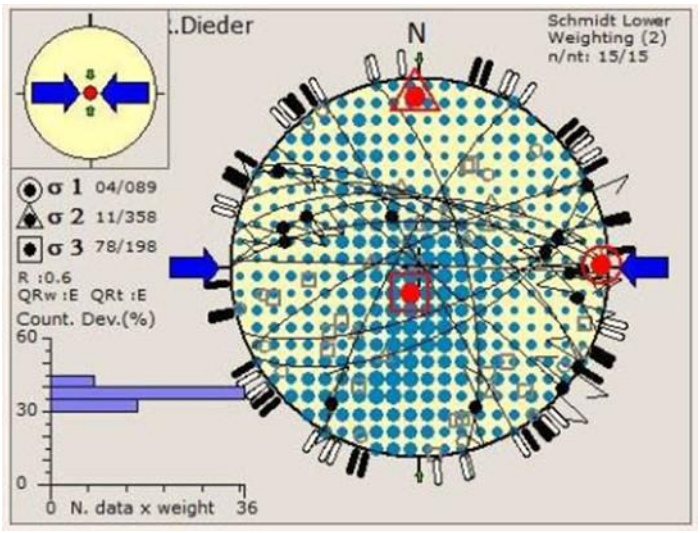

Fig. 9. Stress inversion result for site 4 (stations S10, S11 and S12).

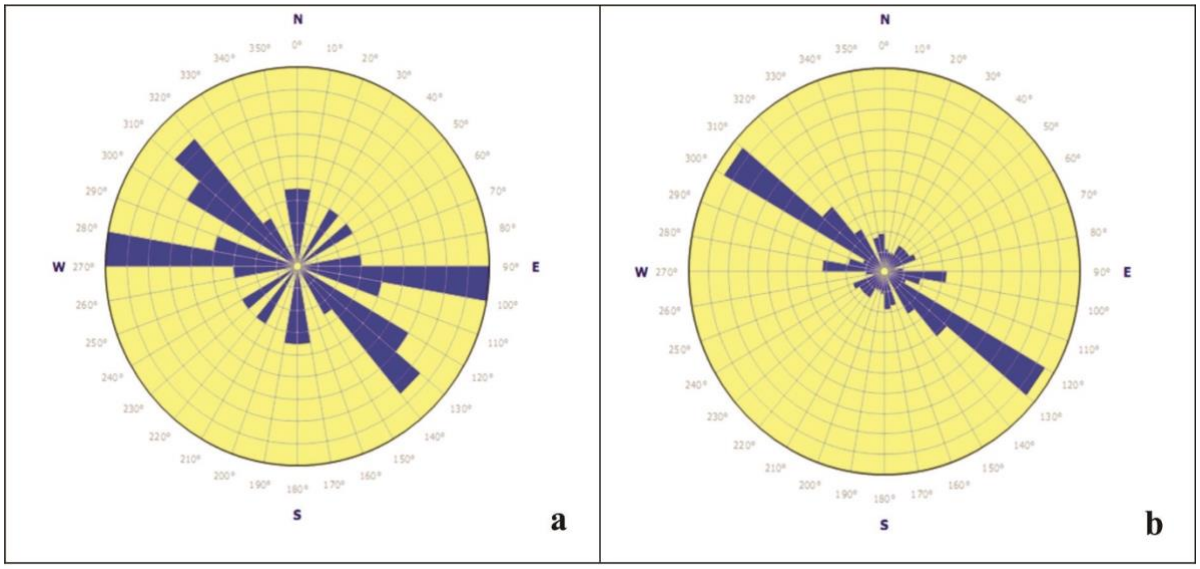

Fig. 10. (a) Rose diagrams of 180 joints in station S11; (b) 150 joints in station S12

5. Discussion

Fault-slip data and joints obtained from the Late Cretaceous rocks (WSL and ASL Formations) are presented as stress tensors' and rose diagrams' orientations and viewed alongside the geological map (Fig. 11). The results derived from the four sites distinguish both extensional and compressive regimes. Based on these inferred paleostress regimes, the area of investigation is split into two different parts. The SW part pertaining to the study area represents stress regimes that are extensive to transtensive whereas the NE part indicates a compressive stress regime. The findings in Site 1 demonstrate that σ_3 (S_{hmin}) is a sub-horizontal oriented NNE-SSW, and the R' value reaches 0.68, therefore, it belongs to a pure extensive regime (Table 1 and Figs. 11 and 12). Instead, the Site 2 stress tensor also shows that σ_3 (S_{hmin}) is sub-horizontal, but the R' value is 0.80, which implies that it belongs to the transtensive regime (Table 1 and Figs. 11 and 12). This indicates that the NNE-SSW extension is account for the E-W to ESE-WNW normal faults and graben-horst structures in the studied area (Figs. 5a, c and d). The extensive and transtensive tensors in this part of the research area can be described as local stresses, which result from a permutation of the principal stress axes, i.e., modifying the σ_1 and σ_2 stress axes during the tectonic events that created the (AHS). This situation can explain as a permutation of stress axes $\boldsymbol{\sigma_1}$ and $\boldsymbol{\sigma_2}$ that occur during tectonic events and partitioned strike-slip deformation. Such changes from predominantly strike-slip to predominantly normal faulting modes ($\boldsymbol{\sigma_1}$/ $\boldsymbol{\sigma_2}$ permutation) frequently occur during a single stage and a distinct stress field. The obtained results are consistent with Neogene extension, as identified in previous studies (e.g., Diabat et al., 2004; Diabat 2009 and 2015; Hardy et al., 2010).

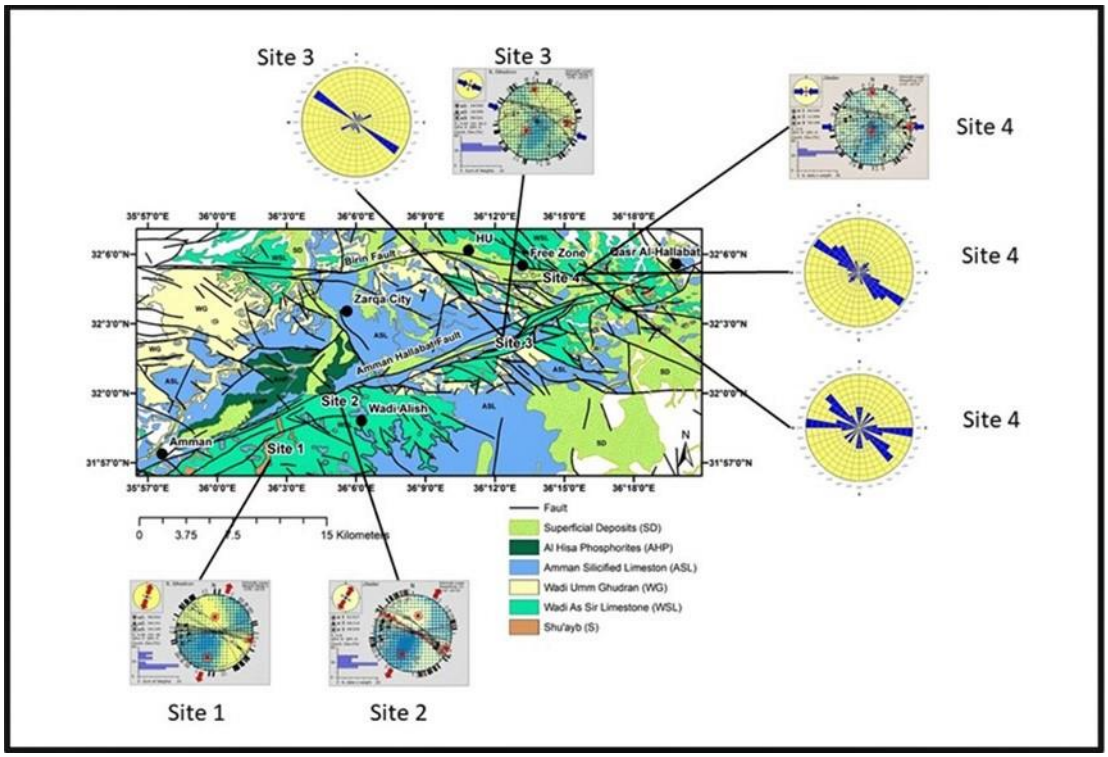

Fig. 11. Geological map with displayed stress tensors and rose diagrams of the orientation data.

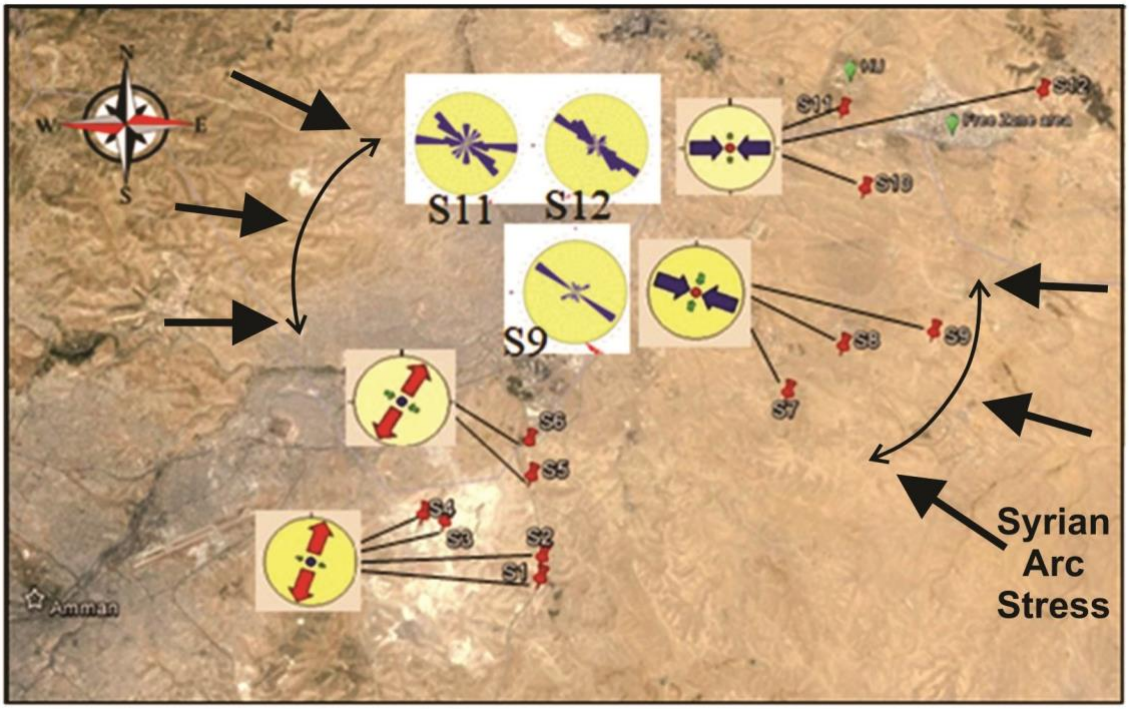

Fig. 12. Tensor solutions and rose diagrams are drawn on a Google Earth photo in the study area. Blue, red and green arrows show the maximum, minimum and intermediate principal stresses, respectively. The fluctuation of the Syrian arc stress in the are also indicated.

Site 3 in the NE portion of the study area indicates that σ1 (S_{Hmax}) is sub-horizontally oriented ESE-WNW and the R' value is 2.65, indicating that it belongs to the pure compressive regime (Table 1 and Figs. 11 and 12). In addition, at Site 4, the stress tensor reveals that σ1 (S_{Hmax}) is sub-horizontally orientated E-W with an R' value of 2.60, indicating that it is formed due to a pure compressive regime (Table 1 and Figs. 11 and 12). Additionally, there is a noticeable bend to the right of the Amman Hallabat fault here (Fig. 3). This resulted in certain compressional structures due to local transpressive stress. The obtained findings are consistent with the (SAS) in the Late Cretaceous (Turonian) to Miocene (e.g., Eyal and Reches 1983; Zain Eldeen et al., 2002). Our findings indicate that S_{Hmax} fluctuated between the E-W and ESE-WNW directions, whereas SHmin was normal to the compression directions and oriented NNE-SSW (Table 2 and Fig. 12).

The findings of the fault-slip data's stress inversion are assembled at four sites and reveal both compressional and extensional regimes. Accordingly, the findings that are obtained from the southwestern part of the area of investigation demonstrate that σ_2 (S_{Hmax}) and σ_3 (S_{hmin}) are sub-horizontal where σ_1 is sub-vertical through two stress tensors (e.g., Sites 1 and 2). Further, their R' values ranged between 0.68-and 0.80. Hence, both tensors refer to pure transtensive and extensive regimes such that σ_3 swings throughout the NNE-SSW (Table 1 and Fig. 12). In the northeastern part of the area of investigation, σ_3 is sub-vertical and σ_1 (S_{Hmax}) is sub-horizontal, and their R' values are ranged between 2.60-2.65, indicating a compression regime in which the direction of the maximum compression (σ_1) swings around E-W (Table 1 and Fig. 12). The study area's spatial difference related to the stress regime type (Fig. 12), which includes the eastern part of the main (AHF), is consistent with previous studies, which claim that NW compressional stresses acted on the area and formed the main (AHF). This fault changes direction repeatedly along its strike, including being associated with a vertical slip component from either transpression or transtension outside the investigation area.

Table 2. A summary of the time constraints for determining paleostress directions in the Dead Sea Rift region.

Series	Eyal and Reches (1983)	Ron and Eyal (1985)	Eyal (1996)	Badawy and Horvath (1999)	Zain Eldeen et al. (2002)	Diabat (2015)
Holocene (Present-day stress field)			(SAS) ESE-WNW S_{Hmax}	NW-SE S_{Hmax}	NW-SE (Present-day S_{Hmax}	
Post-Pleistocene		N-S S_{hmin}			T7: E-W S_{Hmax} T6: N-S S_{Hmax}	E-W S_{Hmax}
Miocene/ Pleistocene (DSS)	NNW-SSE to N-S S_{Hmax}		NNW-SSE to N-S S_{Hmax}		T5: NNW-SSE to N-S S_{Hmax}	
Miocene (DSS)	NW-SE S_{Hmax}				T4: NW-SE S_{Hmax}	WNW-ESE S_{Hmax}
Late Cretaceous (SAS)	E-W to ESE-WNW S_{Hmax}		ESE-WNW S_{Hmax}		T3: E-W S_{Hmax}	ESE-WNW S_{Hmax}

Additional observations emerge from the interpretations of the associated rose diagrams. The main joint trend at Station S9 is aligned WNW-ESE and is sub-parallel to the maximum compressive stress axis (σ_1) in Site 3 (Fig. 12). This indicates that most joints are of Mode I tensional fractures. In Site 4, the major trend of the joints in Station S11 is E-W, which is sub-parallel to the maximum compressive stress axis (σ_1) (Fig. 12), again, indicating that most joints are of Mode I tensional fractures. The minor

joints' trend at Station S11 and the main joints' trend in S12 consist of a sub-parallel orientation related to the NW-SE, where an acute angle is produced with the maximum compressive stress axis (σ_1) of the same site. These conjugate fractures indicate shearing mode fractures.

6. Conclusions

The new structural findings demonstrate that the northeastern portion of the research area is influenced by compressive stresses in which σ1 swings from E-W to ESE-WNW in response to the (SAS) during the Late Cretaceous. In contrast, the southeastern part of the research area is affected by local stresses, which impose pure transtensive and extensive regimes (Table 1 and Fig. 12). These findings are consistent with either Neogene extension, as proposed in previous research (e.g., Hardy et al., 2010; Diabat 2015), or with a perturbation of the σ1 and σ2 stress axes during the main tectonic event that produced the AHS. In conclusion, the studied area can be subdivided into two sectors based on the resulted paleostress regimes: a SW sector dominated by extensional to transtensive stress regimes which can be explained as a splay of a sinistral Wadi Araba fault (the southern part of the Dead Sea Transform) that bends to the right, and that form a permutation of stress axes σ1 and σ2 occur during that tectonic event and partitioned strike-slip deformation. Such changes from predominantly strike-slip to predominantly normal faulting modes (σ1/ σ2 permutation) frequently occur during a single stage and a distinct stress field. Furthermore, the ESE compression stress is found to be consistent with the NNW-SSE Neogene extension. The NE sector was associated with a Syrian Arc Stress Field orientated E-W to ESE-WNW throughout the late Cretaceous. According to the results of the fracture analysis, there are two main types of joint sets within the area of the study: shear and extensional. In addition, both kinds of fractures are consistent with the data on fault slips and the direction of inferred stress.

Acknowledgements

The authors would like to express their gratitude to Hashemite University's Deanship of Scientific Research for financing this study. Furthermore, the authors wish to express their gratitude to Prof. Iain Stewart, Professor of Geoscience at the University of Plymouth, for his critical reading of the manuscript.

References

Abd, A., 2021. Study of earthquake and flood hazards of Khanaqin-Abbasan NE Iraq using Remote Sensing and GIS Techniques, Ph.D. Thesis, University of Baghdad, Iraq.

Abed, A., 2017. Geology, Environment and Water of Jordan, 2nd edn, Dar Wael, Amman, Jordan.

Abu-Qudaira, M., 2001. The geology of Zarqa map sheet No. 3254 III, and geological map at a scale of 1: 50000, National Geological Mapping Project, Natural Resources Authority, Amman, Jordan.

Abutaha, S., Atallah, M., Abed, A., 2019. Structural evolution of Wadi Hudaydun in Wadi Shueib Area, NW Jordan. Jordan Journal of Earth and Environmental Sciences, 10(3), 152-160.

Ahmad, F., Farouk, S., Abdel Moghny, M.W., 2014. A regional stratigraphic correlation for the upper Campanian phosphorites and associated rocks in Egypt and Jordan. Proceedings of the Geologists' Association,1 25, 419-431.

Al Hiyari, A., 2004. The geology of Qasr Al Hallabat map, sheet No 3254 II and Geological map at a scale 1:50000 Geol Mapping Project, Nat Res Authority, Amman, Jordan.

Al Hseinat, M., Al-Rawabdeh, A., Al-Zidaneen, M., Ghanem, H., Al-Taj, M., Diabat, A., Jarrar, G.,Atallah, M., 2020. New insights for understanding the structural deformation style of the strike-slip regime along the Wadi Shueib and Amman-Hallabat Structures in Jordan based on remote sensing data analysis, Geosciences, 10, 253.

Alawabdeh, M., Perez-Pena, J., Azanon, J., Booth-Rea, G., Atallah, M., Galve, J., 2016. Stress analysis of NW Jordan: New episode of tectonic rejuvenation related to the Dead Sea transform fault. Arabian Journal of Geosciences, 264, 1-11.

Al-Khatib, N., Atallah, M., Diabat, A., 2010. Paleostress analysis of the Cretaceous rocks in northern Jordan. Jordan Journal of Earth and Environmental Sciences, 3, 25-36.

Al-Shwaily, A., Al-Obaidi, M., 2019. Paleostress analysis of Neogene rocks in Zurbatiyah area, E Iraq. Iraq Bulletin of Geology and Mining, 15(1), 43-57.

Al-Taj, M., Atallah, M., Abed, A., 2004. Fractures associated with the Dead Sea transform fault in the Jordan Valley, Jordan. Abhath Al-Yarmouk Series of Basic Sciences and Engineering, 19B, 7-21.

Angelier, J., 1994. Fault slip analysis and paleostress reconstruction. In: Hancock, P. (eds), Continental defamation, Pergamon, Oxford, 53-100.

Atallah, M., 1992. Tectonic evolution of northern Wadi Araba, Jordan. Tectonophysics, 204, 17-26.

Atallah, M., Mikbel, S., 1992. Structural analysis of the folds between Wadi El Yabis and the basalt plateau, northern Jordan. Dirasat, 19B, 43-58.

Badawy, A., Horvath, F., 1999. The Sinai subplate and tectonic evolution of the northern Red Sea region. Journal of Geodynamics, 27, 433-490.

Bott, M., 1959. The mechanisms of oblique slip faulting. Geology Magazine, 96, 109-117.

Delvaux, D., 2011. Win-Tensor, an interactive computer program for fracture analysis, crustal stress reconstruction, EGU General Assembly, Geophysical Research Abstract.

Delvaux, D., Sperner, B., 2003. Stress tensor inversion from fault kinematic indicators and focal mechanism data: the TENSOR program. In: New Insights into Structural Interpretation and Modelling (D. Nieuwland Ed.). Geological Society, London, Special Publications, 212, 75-100.

Delvaux. D., Moeys, R., Stapel, G., Melnikov, A., Ermikov, V., 1995. Paleostress reconstructions and geodynamics of the Baikal region, central Asia, Part I, Paleozoic and Mesozoic pre-rift evolution. Tectonophysics, 252, 61-101.

Diabat, A., 2009. Structural and Stress analysis based on fault-slip data in the Amman area, Jordan. Journal of African Earth Sciences, 54, 155-162.

Diabat, A., 2015. Structural and Stress Analysis of the Area between Al-Akeider and Mughayer As-Sirhan, Northwestern Badia-Jordan. Jordan Journal of Earth and Environmental Sciences, 7(1), 37-48.

Diabat, A., Abdelghafoor, M., 2004. The geology of Amman map sheet No 3253 I, and geological map at a scale of 1: 50,000, National Geological Mapping Project, Natural Resources Authority, Amman, Jordan.

Diabat, A., Masri, A., 2005. Orientation of the principal stresses along Zerqa–Ma'in Fault, Jordan. Mu'tah Lil-Buhuth wad-Dirasat, 20, 57-71.

Diabat, A., Atallah, M., Salih M., 2004. Paleostress analysis of the Cretaceous rocks in the eastern margin of the Dead Sea Transform. Journal of African Earth Sciences, 38, 449-460.

Eyal, Y., 1996. Stress fluctuations along the Dead Sea rift since the Middle Miocene. Tectonics, 15, 157-170.

Eyal, Y., Reches, Z., 1983. Tectonic analysis of the Dead Sea rift region since the Late Cretaceous based on mesostructures. Tectonics, 2, 167-185.

Faddah, E., 1988. The geology of Sahab map sheet No 3253 IV, and geological map at a scale of 1: 50000, National Geological Mapping Project, Natural Resources Authority, Amman, Jordan.

Farouk, S., Ahmad, F., Powell, J., Marzouk, A., 2016. Integrated microfossil biostratigraphy, facies distribution and depositional sequences of the upper Turonian to Campanian succession in northeast Egypt and Jordan. Facies, 62, 8.

Farouk, S., Ahmad, F., Powell, J., 2017. Cenomanian–Turonian stable isotope signatures and depositional sequences in northeast Egypt and central Jordan. Journal of Asian Earth Sciences, 134, 207–230.

Farouk, S., Marzouk, A.M., Fayez, A., 2014. The Cretaceous / Paleogene boundary in Jordan. Journal of Asian Earth Sciences. 94, 113–125.

Ferry, M., Meghraoui, M., Abou Karaki, N., Al-Taj, M., Amoush, H., Al-Dhaisat, S., Barjous M., 2007. A 48-kyr-long Slip rate history for the Jordan Valley segment of the Dead Sea Fault. Earth and Planetary Science Letters, 260, 394-406.

Galli, P., 1999. Active tectonics along the Wadi Araba–Jordan Valley transform fault. Journal of Geophysical Research, 104, 2777-2796.

Garfunkel, Z., 1981. Internal structure of the Dead Sea leaky transform (rift) in relation to plate kinematics. Tectonophysics, 80, 81-108.

Garfunkel, Z., 1997. The history and formation of the Dead Sea basin. In: Niemi T, Ben-Avraham Z, Gat J (eds.), the Dead Sea: The Lake and its Settings, Oxford University Press, New York, 36-52.

Garfunkel, Z., 2014. Overview of geological features of the Dead Sea Transform. In: Garfunkel Z, Ben-Avraham, Z., Kagan, E. (eds.), the Dead Sea Transform Springer, Dordrecht, 109-150.

Guiraud, M., Laborde, O., Philip, H., 1989. Characterization of various types of deformation and their corresponding deviatoric stress tensors using microfault analysis. Tectonophysics, 170, 89-316.

Hardy, C., Homberg, C., Eyal, Y., Barrier, E., Muller, C., 2010. Tectonic evolution of the southern Levant margin since Mesozoic. Tectonophysics, 494, 211-225.

Masri, M., 1963. Report on the geology of the Amman-Zarqa area Central Water Authority, Amman, Jordan.

Mikbel, S., Zacher, W., 1981. Fold structures in northern Jordan. Neues Jahrbuch für Geologie und Paläontologie Monatshefte, 4, 248-256.

Mikbel, S., Zacher, W., 1986. The Wadi Shueib structure in Jordan. Neues Jahrbuch für Geologie und Paläontologie, Monatshefte, 9, 571-576.

Quennell, A., 1958. The structure and evolution of the Dead Sea Rift. Quaternary Journal of the Geological Society, 64, 1-24.

Quennell, A., 1959. Tectonics of the Dead Sea Rift, International Geological Congress 20th Association of African Geological Surveys, Mexico City, Mexico.

Radaideh, O., Melichar, R., 2015. Tectonic paleostress fields in the southwestern part of Jordan: New insights from the fault slip data in the southeastern flank of the Dead Sea Fault Zone. Tectonics, 34, 1863-1891.

Ron, H., Eyal, Y., 1985. Intraplate deformation by block rotation and mesostructures along the Dead Sea transform, northern Israel. Tectonics, 4, 85-105.

Rowland, S., Duebendorfer, E., Schiefelbein, I., 2007. Structural Analysis and Synthesis-a laboratory course in structural geology. Blackwell Publishing Ltd., USA,

Soumaya, A., Ben Ayed, N., Rajabi, M., Meghraoui, M., Delvaux, D., Kadri, A., Ziegler, M., Maouche, S. Braham, A., 2018. Active faulting geometry and Stress pattern near complex strike-slip system along the Maghreb region: constraints on active convergence in the Western Mediterranean. American Geophysical Union Publications.

Tiwari, S., Beniest A., Biswal, T., 2020. Extension driven brittle exhumation of the lower-middle crustal rocks, a paleostress reconstruction of the Neoproterozoic Ambaji Granulite, NW India. Journal of Asian Earth Sciences, 195, 1-43.

Weber, M., Abu-Ayyash, K., Ben-Avraham, Z., Choi, S., Darwish, J., El-Kelani, R., Garfunkel, Z., Götze, H., Hofstetter, R., Koulakov, I., Lask, G., Mechie, J., Meyer, U., Mohsen, A., Petrunin, A., Rioseco, E., Ryberg, T., Rümpker, G., Sobolev, S., 2014. Geophysical studies of the lithosphere along the Dead Sea Transform. In: Garfunkel, Z.Ben Avraham, Z. (eds.), the Dead Sea Transform, Springer, Heidelberg, 29-52.

Zain Eldeen, U., 2011. Paleostress reconstructions of Jabal Hafit structures, Southeast of Al Ain City, UAE. Journal of African Earth Sciences, 59, 323-335.

Zain Eldeen, U., Delvaux, D., Jacobs, P., 2002. Tectonic evolution in the Wadi Araba Segment of the Dead Sea Rift, Southwest Jordan. EGU Stephan Mueller Special Publication Series, 2, 63-81.